J. Ind. Geophys. Union, 29(2) (2025), 115-123

Genesis of metastable marcasite phase and associated pyrite in the Proterozoic lamprophyre dyke, Nellore Schist Belt, Southern India

Tushar Meshram[1]* and Srinivasa Rao Baswani[2]
[1]Regional petrology laboratory, Geological Survey of India, Nagpur-440006, India
[2]Regional petrology laboratory, Geological Survey of India, Hyderabad-500068, India
*Corresponding Author: tusharmeshram2911@gmail.com

ABSTRACT

Marcasite is a metastable phase in iron-sulphide solution. If, preserved, it can be used as a significant indicator phase to understand the physio-chemical condition of its formation and associated sulphide system within ore deposits. The present study reports marcasite within the Proterozoic lamprophyre dyke, intruded into the amphibolite of Nellore Schist Belt, Southern India. Marcasite commonly occurs in association with pyrite, chalcopyrite and pyrrhotite in different textural associations. It shows development along the rim and fracture as an alteration of pyrrhotite at places forming characteristic bird eye structure. Pyrite forms later than marcasite, typically occurring along the boundary between marcasite and pyrrhotite. The formations of both marcasites followed by pyrite in the lamprophyre, suggest >l00 ºC and <240 ºC temperature, at low pH during the replacement of pyrrhotite through dissolution-reprecipitation-process under the influence of sulphur-rich hydrothermal solutions. However, the presence of both phases in different textural associations, reveals that the formation conditions of both the Fe sulphide phases i.e. pyrite and marcasite polymorphs are of neutral to alkaline solutions and have an influence on both hydrothermal as well as alkaline parental rock signatures.

Keywords: Pyrite, Marcasite, Pyrrhotite, Lamprophyre, Nellore Schist Belt, Dharwar craton.

INTRODUCTION

The two polymorphs of iron disulfide (FeS_2) are represented by pyrite (cubic) and marcasite (orthorhombic). Marcasite is metastable as compared to pyrite and formed by the alteration of a monosulfide phase like mackinawite or pyrrhotite. Marcasite formation is favoured by low pH on sulfur geochemistry (Goldhaber and Reynolds, 1979). The low-T weathering of pyrrhotite yields FeS_2 (pyrite and marcasite) with a typical replacement textures (especially bird's eye) (Ramdohr, 1975). The main loss of iron from pyrrhotite and its highly porous nature is responsible for its transformation into marcasite and pyrite (Kelley and Turneaure, 1970; Fleet, 1978). In contrast, marcasite to pyrite conversion occurs around 157 and 331°C Temp. at sulfur fugacities buffered and represented by the pyrite-pyrrhotite assemblage (Rising, 1973). Likewise, Qian et al. (2011) explained pyrrhotite to pyrite and marcasite replacement under low temperature (up to 220 °C) hydrothermal conditions. The recent experimental studies by Yao et al. (2020) and Yao (2021) reveal the fast conversion of marcasite to pyrite at higher-temp above 300 °C that restricted the presence of marcasite in the geological records. Although marcasite has a large range of temperatures from >300 ºC e.g. black smokers (Graham et al., 1988) to a lower range <160 ºC (Rising, 1973). Furthermore, the marcasite associated with the mineralization of supergene origin has below pH5 at 25ºC (Murowchick and Barnes, 1986). Likewise, several studies explain the formation of marcasite around temperatures ranging from 80°C to 350°C in various deposits (Barnes, 1979; Anderson and Macqueen, 1982; Ohmoto et al., 1983; Hayba et al., 1985). Especially, the gold is associated with viz-a-viz hosted by pyrite and marcasite (Cook and Chryssoulis, 1990; Large et al., 2007, 2016; Rickard and Luther, 2007; Deditius et al., 2014; Kusebauch et al., 2019; Wu et al., 2019; Xing et al., 2019) in hydrothermal deposits.

Nevertheless, intergrowth of pyrrhotite-pyrite-marcasite is also common in sedimentary settings (Ruppert et al., 2005; Schieber, 2007, 2011), associated with the epithermal system (Franchini et al., 2015; Rottier et al., 2016), Carlin as well as orogenic gold deposits (Fleet and Mumin, 1997; Cline, 2001; Teal and Jackson, 2002; Emsbo et al., 2003; Muntean et al., 2011; Soares et al., 2018; Stromberg et al., 2019), in supergene deposits (Petersen, 1965; Kelly and Turneaure, 1970; Nickel et al., 1974; Einaudi, et al., 2003), VHMS deposits (Maslennikov et al., 2013; Tessalina et al., 2017; Essaifi et al., 2019), and mineralization associated with hydrothermal vent in deep sea (Goldfarb, 1983; Koski et al., 1984; Hannington and Scott, 1987; Schoonen and Barnes, 1991*a*, *b*, *c*; Goldfarb et al., 2005). Its predominance is also reported from late-stage epithermal systems associated with hydrothermal breccias related mineralization e.g. Agua Rica deposit, Argentina (Franchini et al., 2015).

In neutral to alkaline solutions polysulfides are stable at <240°C (Giggenbach, 1974; Schoonen, 1989). Several studies have explained the presence of pyrite and marcasite under hydrothermal conditions (Schoonen and Barnes, 1991a,b,c; Murowchick, 1992; Qian et al., 2011), and supported marcasite formation under acidic conditions (pH <5), or in S(-II)-deficient solutions (saturation index << 1000 concerning either pyrite or marcasite). In contrast, pyrite generation is at relatively higher pH or S(-II)-rich solutions with saturation index >1000 (for either pyrite or marcasite) (Murowchick and Barnes, 1986; Qian et al., 2011). The occurrence of marcasite is a useful indicator of low-temperature environments

(Schoonen and Barnes, 1991a, b, c; Qian et al., 2011 and references therein).

In the present study, we discuss the mutual textural association of pyrrhotite, pyrite, and marcasite that occur in calc-alkaline lamprophyre intruded in the southern part of the Nellore Schist Belt. This lamprophyre is intruded by the minor quartz veins that generally carry sulfide mineralization. The lamprophyre dyke have developed under the influence of the hydrothermal system in the Nellore Schist Belt and the Eastern Dharwar Craton. Here, we present the formation of marcasite from the replacement of pyrrhotite in lamprophyre, to ascertain its role in the formation of base-metal mineralization in the area and its regional implication.

GEOLOGY OF THE AREA

The Dharwar Craton represented one of the prominent Archean cratons of the Indian shield located in southern India which can be divided into eastern Dharwar and western Dharwar cratons with the boundary demarcated by N-S trending Closepet granite. The eastern Dharwar Cratons is covered by the granite/gneisses/TTGs of Neoarchean age with the presence of NNW-SSE trending greenstone belts (Chadwick et al., 2000; Jayananda et al., 2000). The study area is located in the eastern Dharwar Cratons and close to the vicinity of the contact zone of Neoarchean Nellore Schist Belt and Eastern Ghats Belt. Nellore Schist Belt subdivided into Udayagiri and Vinjamuru groups, are situated juxtaposed to Nallamalai Fold belt and Cuddapah basin having thrust contact (Figure 1c) (Saha, 2011; Meshram et al., 2021, 2022). The Vinjamuru group predominantly contain metasedimentary rocks composed mainly of phyllites and quartzites along with the subordinate volcanics. Whereas, Udayagiri group is dominantly composed of amphibolite/meta-basalt.

The reported lamprophyre with sulfide mineralization is situated in the southern most extent of the NSB (Meshram et al., 2021, 2022) (Figure 1a-c). The studied lamprophyre is 2.3 Ga old, intruded into amphibolites of Udayagiri domain and it has taken part in the deformation and metamorphic processes associated with the Nellore Schist Belt (Figure 2a) (Meshram et al., 2021). It also exhibits late hydrothermal imprints represented by mineralized sulphide -rich quartz veins. There are number of quartz veins associated with sulfide mineralization which intruded along the Nellore Schist Belt (Figure 2b). The Garimanipenta, Venkatadripalem, Masayapeta and Tirumalapuram areas are well-known for potential sulphide mineralized occurrences along Nellore Schist Belt, which has been explored by the Geological Survey of India. This sulphide occurrence is situated almost 80 km north of the lamprophyre of the study area.

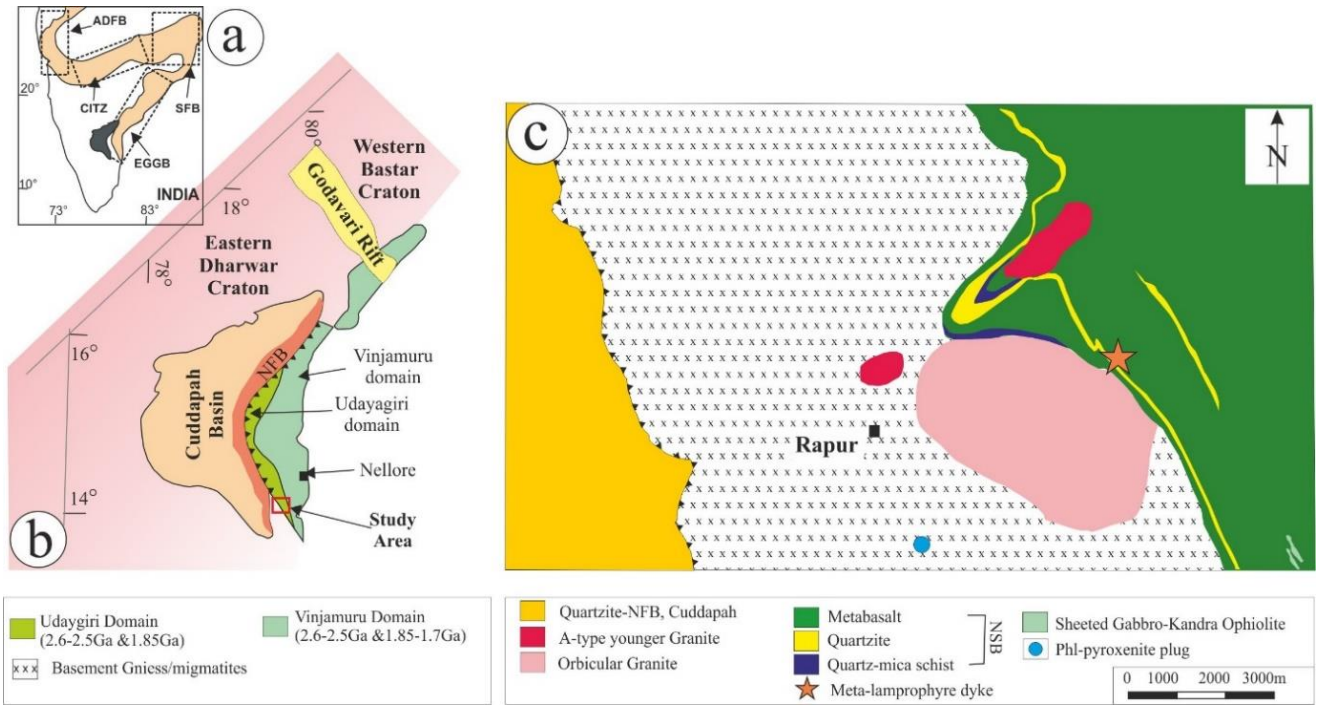

Figure 1. **(a)** Inset map of India showing location of Cuddapah basin. **(b)** Regional geological map showing location of study area in the Eastern Dharwar Craton and its relationship with the Cuddapah basin, Nellore Schist Belt and Nalamallai Fold Belt (NFB). **(c)** Study area showing the location of lamprophyre within Udayagiri meta-basalt (after Meshram et al., 2021, 2022).

PETROGRAPHICAL STUDY

The lamprophyre is foliated in nature and shows preferred orientation of amphibole and feldspar and secondary quartz along with sulphides (Figure 2b and Figure 3a,b). Detailed petrographical studies reveal the presence of primary porphyritic to panadiomorphic textures. The phenocryst phase is predominantly represented by phlogopite set in the fine-grained groundmass (Figure 3a,b). It contains principal sulphide minerals like pyrrhotite, marcasite, pyrite and chalcopyrite in association with silicates. The marcasite shows pale yellowish colour compared to pyrite and show anisotropism in shades of light yellow (Figure 3c-e). The marcasite veinlets have a thickness of a few cm, and occur in association with the pyrrhotite. It forms criss-cross veinlets, develops along fractures, and rims of the grain boundaries (Figure 3f). Pyrrhotite appears as grains up to a few centimeters in diameter, with all grains replaced by marcasite. Marcasite seams are consistently found along the borders of pyrrhotite grains. In some areas, pyrite occurs as euhedral grains up to a few millimeters in diameter, embedded within marcasite.The chalcopyrite grains in the lamprophyre do not show any alteration and sharp contact with both pyrrhotite and marcasite. Limonite/siderite of a reddish-brown colour is seen under transmitted light.

The replacement textures show development of remiform borders of marcasite, whereas, formation of tiny rounded to spheroids shapes with double marginal zone is more common and significant. A worm-like body of marcasite along pre-existing microfissures, such as cracks and cleavage planes in the original pyrrhotite, is also observed. At places, a series of concentric layers of marcasite (bird's-eye structures, (Figure 3e, f), are separated from each other by open voids, and finally the whole pyrrhotite grain is transformed to marcasite. Pyrrhotite is showing skeletal texture due to the replacement of entire grains by marcasite.

MINERAL CHEMISTRY OF PYRRHOTITE, CHALCOPYRITE AND PYRITE

A total of 28 EPMA spot analyses were carried out, on the pyrrhotite 12 numbers (nos.), chalcopyrite 06 nos., marcasite 05 nos. and pyrite 05 nos. The instrument was set under 15 kV accelerating voltage, one μm beam diameter, and 20 nA beam current for the measurements. The counting times for peak and background were the 40 s and 20 s, respectively. The precisions of the analyses were ±0.5% element concentrations. The ZAF matrix corrections were carried out using the CAMECA supplied Peak sight program. The major element compositions are listed in Tables 1-3. The general representation is shown in the binary plot S against Cu+Fe in Figure 4a and also plotted Fe and S variation in box plot (Figure 4b). They show systematic variation in copper, iron and sulphur.

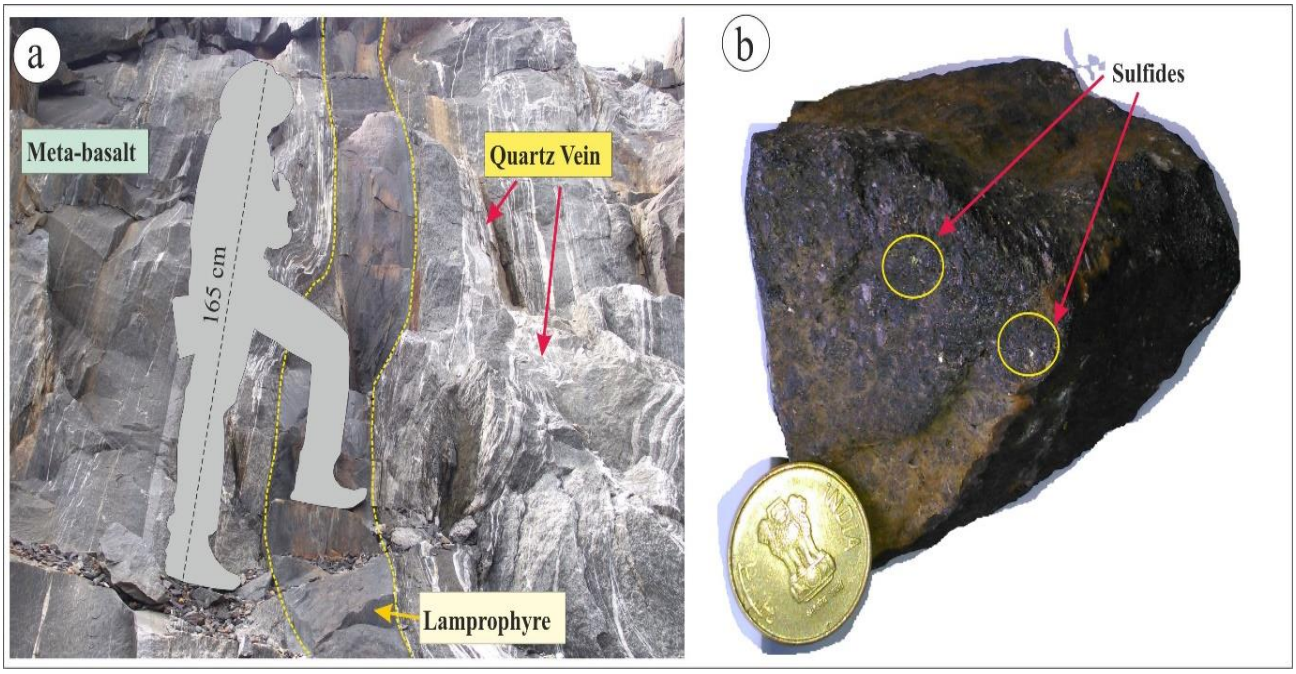

Figure 2. (a) Field photograph showing the lamprophyre intruded within Udayagiri meta-basalt, Note-extensive intrusion of intense quartz veining parallel to the lamprophyre intrusion. **(b)** Close-up view photograph showing porphyritic texture in lamprophyre with the presence of sulfide mineralization (Location: quarry section west of Rapuru near Gilakapadu area)

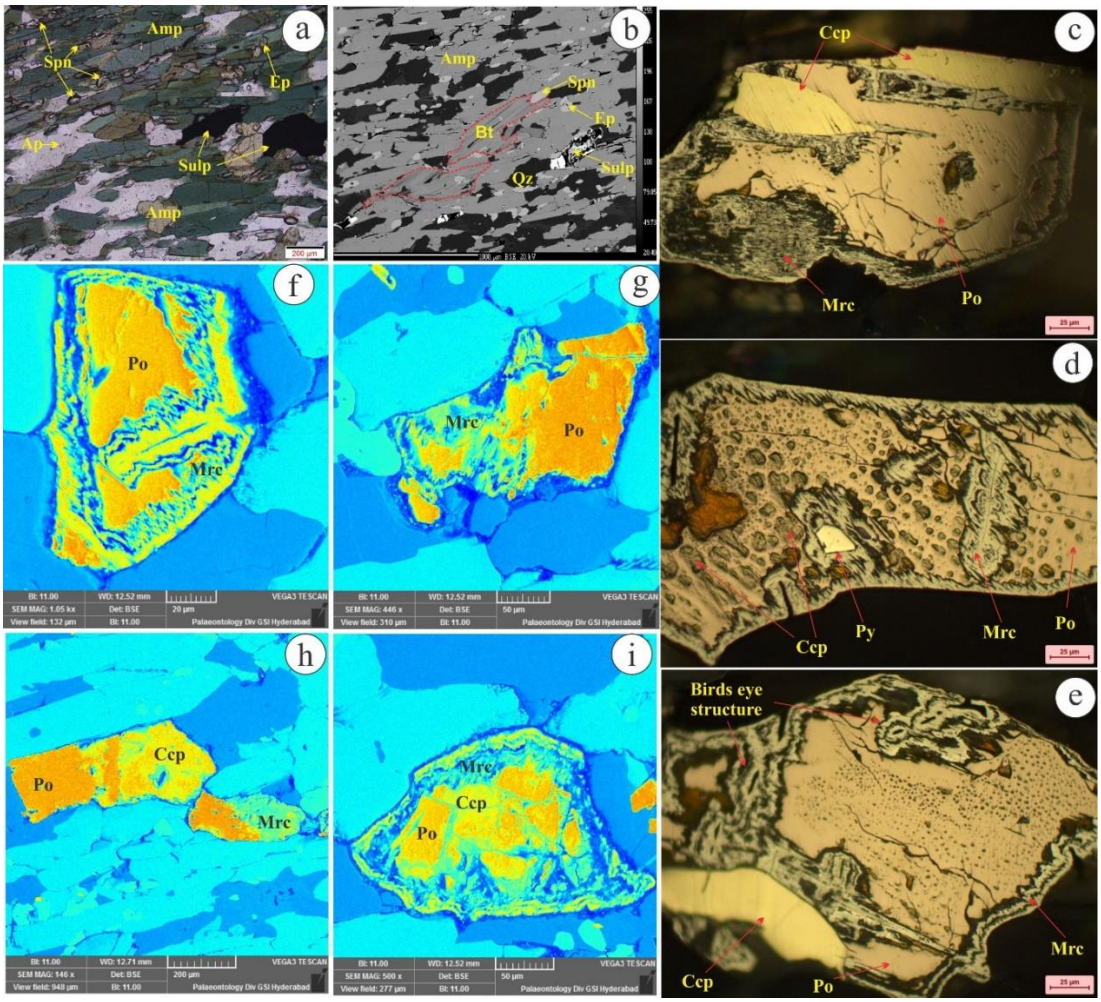

Figure 3. **(a)** Photomicrograph showing presence of sulphide along the foliation plane within lamprophyre; note- alignment of amphibole defining foliation. **(b)** Back scattered electron image showing presence of sulphide and its replacement within lamprophyre. **(c)** Photomicrograph showing replacement of pyrrhotite with the marcasite and formation of chalcopyrite. **(d)** Photomicrograph showing replacement of pyrrhotite to marcasite and formation of chalcopyrite as inclusion along with late phase pyrite. **(e)** Photomicrograph showing replacement of pyrrhotite to marcasite with development of characteristic birds eye structure. **(f-i)** False color composite images illustrate the various textural associations of pyrrhotite replacement by marcasite, along with the formation of chalcopyrite and pyrite.

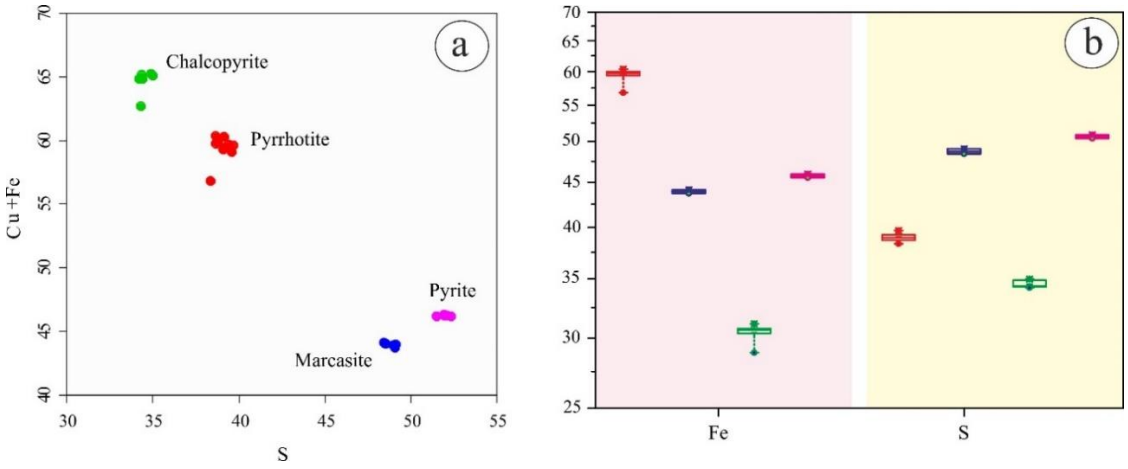

Figure 4. **(a)** Binary variation plot of S against Cu+Fe. **(b)** box plot for pyrite-chalcopyrite-pyrrhotite and marcasite show behaviour of Fe and S.

In general, pyrrhotite contains 56.78–60.63 wt% Fe (average 59.51 wt%), 38.33–39.68 wt% S (average 38.99 wt%), with higher concentrations of Ni, Co, and Mo, while the remaining elements are below detection limits. Chalcopyrite has 28.89–31.13 wt% Fe (average 30.40 wt%), 34.20–34.98 wt% S (average 34.51 wt%), and 33.81–34.45 wt% Cu (average 34.25 wt%), with higher levels of Mo and the remaining elements below detection limits. Pyrite shows 46.09–46.31 wt% Fe (average 46.20 wt%), 51.10–51.94 wt% S (average 51.45 wt%), and 0.009–0.076 wt% Cu, with other elements either insignificant or below detection limits. Marcasite contains 43.71–44.11 wt% Fe and 48.43–49.07 wt% S, with higher concentrations of Ni, Co, and Mo, while the remaining elements are below detection limits.

Table 1. Representative EPMA analysis of Pyrrhotite from meta-lamprophyre dyke.

Point	1 / 1	2 / 1	3 / 1	6 / 1	7 / 1	9 / 1	11 / 1	12 / 1	13 / 1	15 / 1	16 / 1	20 / 1
	Pyrrhotite											
Cu	0.037	0	0.101	0.029	0	0	0.021	0.003	0	0	0	0.042
Co	0.258	0.245	0.27	0.256	0.237	0.22	0.265	0.266	0.25	0.22	0.215	0.25
Ni	0.176	0.212	0.231	0.153	0.233	0.246	0.27	0.19	0.262	0.212	0.198	0.217
Fe	59.982	59.863	59.608	56.789	59.11	59.989	59.263	59.625	60.304	59.765	59.462	60.363
Zn	0	0	0	0	0	0.172	0	0.025	0	0.012	0	0.01
S	38.758	38.796	39.38	38.332	39.579	38.771	39.093	39.685	39.134	38.645	39.123	38.65
Te	0.037	0.022	0	0.01	0	0	0	0	0.048	0.036	0.012	0
Au	0	0	0	0	0	0	0	0	0	0	0	0
Mo	0.54	0.636	0.532	0.424	0.643	0.501	0.727	0.681	0.657	0.649	0.661	0.489
Bi	0.143	0.029	0.056	0.279	0.131	0.175	0.051	0.135	0.277	0.086	0.191	0.21
Se	0.013	0.007	0	0.048	0.039	0.003	0.013	0	0	0.015	0.051	0.002
Ag	0.001	0	0	0.031	0	0	0.039	0.026	0	0.035	0	0
Sb	0	0	0	0	0	0	0	0	0	0	0	0
Sn	0	0.042	0.044	0.031	0	0.07	0.029	0.055	0.05	0.01	0.141	0.055
Pb	0.14	0.218	0.097	0.055	0.133	0.266	0.101	0.127	0.062	0.188	0.26	0.153
As	0	0	0	0	0	0	0	0	0	0	0	0.017
Total	100.086	100.07	100.319	96.439	100.104	100.413	99.872	100.817	101.044	99.874	100.314	100.458

Table 2. Representative EPMA analysis of Chalcopyrite from meta-lamprophyre dyke.

Point	4 / 1	5 / 1	8 / 1	10 / 1	18 / 1	19 / 1
	Chalcopyrite					
Cu	34.373	33.813	34.423	34.452	34.1	34.353
Co	0.1	0	0.013	0.017	0.035	0.019
Ni	0	0.039	0	0.008	0.013	0.012
Fe	30.514	28.891	30.749	30.378	31.139	30.756
Zn	0	0.083	0.039	0	0	0.075
S	34.204	34.278	34.34	34.402	34.894	34.98
Te	0.029	0	0	0	0	0
Au	0	0	0	0	0	0
Mo	0.695	0.437	0.587	0.74	0.614	0.621
Bi	0.256	0.024	0.022	0.02	0.142	0.337
Se	0	0.01	0	0.104	0	0
Ag	0	0	0	0	0.078	0
Sb	0	0	0	0	0	0
Sn	0	0.018	0	0.054	0.034	0
Pb	0	0.296	0.141	0.188	0.258	0.083
As	0	0	0	0	0	0
Total	100.172	97.89	100.315	100.363	101.307	101.235

Table 3. Representative EPMA analysis of Marcasite and pyrite from meta-lamprophyre dyke**.**

Point	14 / 1	15 / 1	16 / 1	17 / 1	17 / 1	1 / 1	2 / 1	3 / 1	6 / 1	7 / 1
	Marcasite					Pyrite				
Cu	0	0	0	0	0	0.076	0.024	0.009	0.032	0.029
Co	0.388	0.295	0.312	0.376	0.423	0.034	0.076	0.025	0.044	0.081
Ni	0.765	0.798	0.894	0.889	1.052	0.047	0.021	0.016	0	0.021
Fe	43.714	43.961	43.887	44.065	44.118	46.09	46.22	46.23	46.15	46.31
Zn	0.05	0.031	0	0.045	0	0	0.032	0	0.027	0
S	49.078	49.12	48.976	48.538	48.438	51.48	52.1	51.92	52.32	51.94
Te	0.008	0.005	0	0.006	0	0.024	0	0.083	0	0
Au	0	0	0	0	0	0.009	0	0	0	0
Mo	0.84	0.81	0.79	0.812	0.826	0	0	0	0	0
Bi	0.241	0	0	0	0	0	0	0	0	0
Se	0.036	0.028	0.007	0.031	0.005	0	0	0	0	0
Ag	0	0	0	0	0	0	0.014	0	0.015	0.002
Sb	0	0	0	0	0	0	0	0	0	0
Sn	0.085	0.083	0.057	0.064	0.066	0	0	0	0	0
Pb	0.044	0.03	0.078	0.041	0.304	0	0	0	0	0
As	0	0	0	0	0	0	0	0.006	0	0
Total	95.25	95.161	95.001	94.867	95.233	97.76	98.487	98.289	98.588	98.383

DISCUSSION

Conditions of formation of marcasite

The pyrrhotite-marcasite transformation is common in the supergene zone and association of secondary pyrite with the marcasite may point to higher confining pressures during the transformation process, or to the direct precipitation of pyrite from solution under conditions of high Fe and S activity (Schoonen and Barnes, 1991a,b,c). The transformation of pyrrhotite to marcasite with the presence of chalcopyrite in alkaline rocks in southern India is akin to many ore deposits (e.g., Einaudi, 1971; Fleet, 1970, 1978). The pyrrhotite transformation to marcasite and/or pyrite, also develops large porosity (Murowchick, 1992). Distinct replacement textures of pyrrhotite conversion to either pyrite or marcasite are ilustarted in (Figure 3). During the evolution of solution, the overgrowth and formation of marcasite happened by direct viz-a-viz simultaneous pyrrhotite conversion and their association chalcopyrite reveals the crystal growth of marcasite as a precipitation mechanism from same solution.

The experimental study of Qian et al. (2011) suggested that the pyrrhotite to Fe disulfide reaction supports the dissolution-reprecipitation mechanism under hydrothermal conditions and temperature below 220ºC preferentially at low pH. Schoonen and Barnes (1991a,b,c)'s experimental studies suggest that at < l00ºC, pyrite and marcasite are formed by sulfidation of FeS with polysulfides, and > l00ºC, they are formed via sulfidation with the loss of iron and release of earlier FeS phases. They are only stable in neutral to alkaline solutions < 240°C (Giggenbach, 1974; Schoonen, 1989). The formation of both phases under hydrothermal conditions suggests its genesis in acidic conditions (pH<5), or in S(-II)-deficient solutions while pyrite is formed at relatively higher pH or S(-II)-rich solutions (Murowchick and Barnes, 1986; Schoonen and Barnes, 1991a, b, c; Murowchick, 1992; Qian et al., 2011). Experimental study of Yao (2021) has shown rapid transformation from marcasite to pyrite at higher temperatures (>300 ºC).

It is obvious that the formation of marcasite in alkaline rocks is the replacement of pyrhotite by dissolution-reprecipitation mechanism under hydrothermal conditions and also by enrichment of sulphur from solution through sulfidation processes progressively more sulphur-rich phases pyrite and chalcopyrite. Therefore, the temperature ranges of formations of marcasite in the alkaline rocks are above l00ºC and below 220ºC and replacement of pyrrhotite through dissolution-reprecipitation process under the influence of sulphur rich hydrothermal solutions. In the present study, it is observed that the formation of both pyrite and marcasite indicate similar conditions. However, the presence of both phases in different textural associations reveal that the formational conditions for them are of mixed nature and have the influence of both hydrothermal as well as alkaline parental rock signature. The mineral typically forms under low-temperature, sulfur-rich conditions, often associated with hydrothermal fluids that interact with the host rock. The alkaline environment plays a crucial role in stabilizing marcasite, facilitating its precipitation from the circulating fluids. These fluids, rich in sulfur, promote the replacement of pyrrhotite and other minerals, allowing

marcasite to crystallize in fractures and intergranular spaces. This process often occurs in proximity to base metal mineralization, further indicating the influence of the hydrothermal system in the formation of marcasite.

CONCLUSIONS

The Nellore Schist Belt hosts potential base metal sulphide occurrences along its southern extension. Present study reported the marcasite within the lamprophyre dyke intruded into the amphibolite of Nellore Schist Belt, Rapuru, India. Marcasite commonly occurrs in association with pyrite, chalcopyrite, pyrrhotite in different textural association. Marcasite is metastable phase in iron-sulphide solution significantly used as an indicator phase to understand the physio-chemical conditions of sulphide system associated with ore deposits. The textural evidence shows its development along the rim and fractures as an alteration of pyrrhotite with characteristic bird eye structure. Mutual association of marcasite-pyrite in the lamprophyre is generally restricted to <240ºC temperature, neutral to alkaline solutions at low pH during dissolution-reprecipitation process under the influence of sulphur rich hydrothermal solutions.

Acknowledgement

Authors extend sincere thanks to the Additional Director General, Geological Survey of India, Southern Region Hyderabad for providing the necessary facilities during filed season programme. We are thankful to the Additional Director General, Geological Survey of India, Central Region for according permission to publish this work. The authors also extend their sincere gratitude to an anonymous reviewers for critical scrutiny and constructive suggestions, which immensely helped to improve the manuscript. Finally, the authors are thankful to the Chief Editor for providing an opportunity and kind consideration of our research in the journal.

Author Credit Statement

Tushar Meshram: Conceptualization, field investigation, writing original draft, review and editing. Srinivasa Rao Baswani**:** Conceptualization, field investigation, formal analysis, writing, review and editing

Data availability

All data generated or analysed during this study are included in this article.

Compliance with ethical standards

No conflict of interest and the authors declare that they have no known competing financial interests or personal relationships that could have appeared to influence the work reported in this paper. Adhere to the copyright norms

References

Anderson, G.M. and Macqueen, R. W., 1982. Mississippi Valley type lead-zinc deposits. Geoscience Canada, 9, 108-l17.

Barnes, H.L., 1979. Solubility of ore minerals. Geochemistry of Hydrothermal Ore Deposits, J. Wiley & Sons, 404-454.

Chadwick, B., Vasudev, V.N. and Hegde, G.V., 2000. The Dharwar craton, southern India, interpreted as the result of Late Archean oblique convergence. Precamb. Res., 99, 91–111.

Cline, J.S., 2001. Timing of gold and arsenic sulfide mineral deposition at the Getchell Carlin-type gold deposit, north-central Nevada. Economic Geol., 96(1), 75-89.

Cook, N.J. and Chryssoulis, S.L., 1990. Concentrations of invisible gold in the common sulfides. Canadian Mineral., 28, 1-16.

Deditius, A.P., Reich, M., Kesler, S.E., Utsunomiya, S., Chryssoulis, S.L., Walshe, J. and Ewing, R.C., 2014. The coupled geochemistry of Au and As in pyrite from hydrothermal ore deposits. Geochim. Cosmochim. Acta, 140, 644-670.

Emsbo, P., Hofstra, A.H., Lauha, E.A., Griffin, G.L. and Hutchinson, R.W., 2003. Origin of high-grade gold ore, source of ore fluid components, and genesis of the Meikle and neighbouring Carlin type deposits, northern Carlin trend, Nevada. Economic Geol., 98(6), 1069-1105.

Einaudi, M.T., 1971. The intermediate product of pyrrhotite alteration. American Mineral., 56, 1297–1302

Einaudi, M. T., Hedenquist, J.W. and Inan, E.E., 2003. Sulfidation state of fluids in active and extinct hydrothermal systems: Transitions from porphyry to epithermal environments. Special Publication-Society of Economic Geologists, 10, 285-314.

Essaifi, A., Goodenough, K., Tornos, F., Outigua, A., Ouadjou, A. and Maacha, L., 2019. The Moroccan Massive Sulphide Deposits: Evidence for a Polyphase Mineralization. Minerals, 9(3), 156.

Fleet, M.E. 1970. Structural aspects of the marcasite-pyrite transformation. Canadian Mineral., 10, 225-231.

Fleet, M.E. 1978. The pyrrhotite-marcasite transformation: Canadian Mineral., 16, 31-35.

Fleet, M.E., Mumin, A.H. 1997. Gold-bearing arsenian pyrite and marcasite and arsenopyrite from Carlin Trend gold deposits and laboratory synthesis. American Mineral., 82(1-2), 182-193.

Franchini, M., McFarlane, C., Maydagán, L., Reich, M., Lentz, D. R., Meinert, L. and Bouhier, V., 2015. Trace metals in pyrite and marcasite from the Agua Rica porphyry-high sulfidation epithermal deposit, Catamarca, Argentina: Textural features and metal zoning at the porphyry to epithermal transition. Ore Geol. Rev., 66, 366-387.

Giggenbach, W.F. 1974. Equilibrium involving polysulfide ions in aqueous solutions up to 240°C. Inorganic Chem., 13, 1724-1730.

Goldfarb, M.S., 1983. The genesis of hot spring deposits on the East Pacific Rise 21ºN. The Kuroko and Related Volcanogenetic Massive Deposits. Economic Geology, Monograph 5, 184-197.

Goldfarb, R., Baker, T., Dubé, B., Groves, D.I., Hart, C.J. and Gosselin, P., 2005. Distribution, character and genesis of gold deposits in metamorphic terranes. Society of Economic

Geologists, Economic Geology One Hundredth Anniversary Volume, 407-450.

Goldhaber, M.B. and Reynolds, R.L., 1979. Origin of marcasite and its implications regarding the genesis of roll-front uranium deposits. U.S. Geol. Surv. Standard Report, 1-40.

Graham, U.M., Bluth, G.J., Ohmoto, H., 1988. Sulfide sulfate chimneys on the East Pacific Rise, 11° and 13°N latitudes. Part I: Mineralogy and paragenesis. Canadian Mineral., 26, 487-504.

Hannington, M.D. and Scott, S.D., 1987. Sulfidation equilibria as guides to gold mineralization in volcanogenic massive sulfides. Geol. Soc. America, Abstract 19, 692.

Hayba, D.O., Bethke, P.M., Heald, P. and Foley, N.K., 1985. Geologic, mineralogic, and geochemical characteristics of volcanohosted epithermal precious-metal sulfide deposits. Review in Economic Geology 2, 129-162.

Jayananda, M., Moyen, J.F., Martin, H., Peucat, J.J., Auvray, B. and Mahabaleshwar, B., 2000. Late Archean (2550–2520 Ma) juvenile magmatism in the Eastern Dharwar craton, southern India: constraints from geochronology, Nd–Sr isotopes and whole-rock geochemistry. Precamb. Res., 99, 225–254.

Kelly, W.C. and Turneaure, F.S., 1970. Mineralogy, paragenesis and geothermometry of the tin and tungsten deposits of the eastern Andes, Bolivia. Economic Geol., 65(6), 609-680.

Koski, R.A., Clague, D.A. and Oudin, E., 1984. Mineralogy and chemistry of massive sulfide deposits from the Juan de Fuca Ridge. Geol. Soc.America Bull., 95(8), 930-945.

Kusebauch, C., Gleeson, S.A. Oelze, M., 2019. Coupled partitioning of Au and As into pyrite controls formation of giant Au deposits. Science Advances, 5(5), 1-8.

Large, R.R., Maslennikov, V.V., Robert, F., Danyushevsky, L.V. and Chang, Z., 2007. Multistage sedimentary and metamorphic origin of pyrite and gold in the giant Sukhoi Log deposit, Lena gold province, Russia. Economic Geol., 102(7), 1233-1267.

Large, S.J., Bakker, E.Y., Weis, P., Wälle, M., Ressel, M. and Heinrich, C.A., 2016. Trace elements in fluid inclusions of sediment-hosted gold deposits indicate a magmatic-hydrothermal origin of the Carlin ore trend. Geology, 44(12), 1015-1018.

Maslennikov, V.V., Masslennikova, S.P., Large, R.R., Danyushevsky, L.V., Herrington, R.J. and Stanley, C.J., 2013. Tellurium-bearing minerals in zoned sulfide chimneys from Cu-Zn massive sulfide deposits of the Urals, Russia. Mineral. and Petrol., 107, 67-99.

Meshram, T., Mahapatro, S.N., Aravind, J.K., Dora, M.L., Baswani, S.R., Gopalakrishna, G., Meshram, R., Sesha Sai, V.V., Randive, K. and Das, J., 2021. Geochemistry and Sr-Nd isotopic studies of Palaeoproterozoic (ca. 2.3 Ga) meta-lamprophyre from Rapuru area, Nellore Schist Belt, Southern India: implication for back-arc basin magmatism and its relevance to the Columbia Supercontinent assembly. Geol. Soc. London, Special Publications, 513, 103-132.

Meshram, T., Mahapatro, S.N., Sesha Sai, V.V., Dora, M.L., Randive, K. and Baswani, S.R., 2022. Petrogenesis of phlogopite-pyroxenite from Southern India: implications for the link between Proterozoic subduction- to rift-related arc magmatism. Geosyst. Geoenviron., Volume 1, article id. 100033., DOI: 10.1016/j.geogeo.2022.100033

Muntean, J.L., Cline, J.S., Simon, A.C. and Longo, A.A., 2011. Magmatic–hydrothermal origin of Nevada's Carlin-type gold deposits. Nature Geosci., 4(2), 122.

Murowchick, J.B., 1992. Marcasite inversion and the petrographic determination of pyrite ancestry. Economic Geol., 87, 1141–1152.

Murowchick, J.B. and Barnes, H.L., 1986. Marcasite precipitation from hydrothermal solutions. Geochim. Cosmochim. Acta, 50, 2615-2630.

Nickel, E.H., Ross, J.R. and Thornber, M.R., 1974. The supergene alteration of pyrrhotite pentlandite ore at Kambalda, Western Australia. Economic Geol., 69(1), 93-107.

Ohmoto, H., Mizukami, M., Drummond, S.E., Eldridge, C.S., Pisutha-Arnond, V. and Lenagh, T.C., 1983. Chemical processes of Kuroko formation. In Economic Geology Monograph Series, 5, 570-604.

Petersen, U., 1965. Regional geology and major ore deposits of central Peru. Economic Geol., 60(3), 407-476.

Qian, G., Xia, F., Brugger, J., Skinner, W.M., Bei, J., Chen, G. and Pring, A., 2011. Replacement of pyrrhotite by pyrite and marcasite under hydrothermal conditions up to 220 ℃: An experimental study of reaction textures and mechanisms. American Mineral., 96(11-12), 1878-1893.

Ramdohr, P., 1975. Der erz Mineralien und ihre Verwachsungen: Berlin, Acdemic-Verlag, 173.

Rickard, D. and Luther, G.W., 2007. Chemistry of iron sulfides. Chem. Rev., 107,514-562.

Rising, B.A., 1973. Phase relations among pyrite, marcasite, and pyrrhorite below 300 ℃, Ph.D. thesis, Pennsylvania State University, University Park, Pennsylvania, United State,192p.

Rottier, B., Kouzmanov, K., Wälle, M., Bendezú, R. andFontboté, L., 2016. Sulfide replacement processes revealed by textural and LA-ICP-MS trace element analyses: example from the early mineralization stages at Cerro de Pasco, Peru. Economic Geol., 111(6), 1347-1367.

Ruppert, L.F., Hower, J.C. and Eble, C.F., 2005. Arsenic-bearing pyrite and marcasite in the Fire Clay coal bed, Middle Pennsylvanian Breathitt Formation, eastern Kentucky. Int. J. Coal Geol., 63(1-2), 27-35.

Saha, D., 2011. Dismembered ophiolites in Paleoproterozoic nappe complexes of Kandra and Gurramkonda, South India. J. Asian Earth Sci., 42, 158–175.

Schieber, J., 2007. Oxidation of detrital pyrite as a cause for Marcasite Formation in marine lag deposits from the Devonian of the eastern US. Deep-Sea Res., 54, 1312-1326.

Schieber, J., 2011. Marcasite in black shales - A mineral proxy for oxygenated bottom waters and intermittent oxidation of carbonaceous muds. J. Sediment Res., 81(7), 447-458.

Schoonen, M.A.A., 1989. Mechanisms of pyrite and marcasite formation from solutions between 25 and 300°C. Ph.D. dissertation, Pennsylvania State University, United States, 54-161

Schoonen, M.A.A. and Barnes, H. L., 1991a. Mechanisms of pyrite and marcasite formation from solution: III. Hydrothermal processes. Geochim. Cosmochim. Acta, 55(12), 3491-3504.

Schoonen, M.A.A. and Barnes, H.L., 1991b. Reactions forming pyrite and marcasite from solution: I. Nucleation of FeS_2 below 100 ºC. Geochim. Cosmochim. Acta, 55(6), 1495-1504.

Schoonen, M.A.A. and Barnes, H. L., 1991c. Reactions forming pyrite and marcasite from solution:II. Via FeS precursors below 100 ℃. Geochim. Cosmochim. Acta, 55(6), 1505-1514.

Soares, M.B., Neto, A.V.C., Bertolino, L.C., Alves, F.E.A., de Almeida, A.M., da Silva, P.H.M., de Araujo Mabub, R.O., Manduca, L.G. and de Pamplona Araújo, I.M.C., 2018. Multistage mineralization at the hypozonal São Sebastião gold deposit, Pitangui greenstone belt, Minas Gerais, Brazil. Ore Geol. Rev., 102, 618-638

Stromberg, J.M., Barr, E., Van Loon, L.L., Gordon, R.A. and Banerjee, N.R., 2019. Fingerprinting multiple gold mineralization events at the Dome mine in Timmins, Ontario, Canada: Trace element and gold content of pyrite. Ore Geol. Rev., 104, 603-619.

Teal, L. and Jackson, M., 2002. Geologic overview of the Carlin trend gold deposits. Gold deposits of the Carlin trend. Nevada Bureau of Mines and Geology, Society of Economic Geologists, Bull., 111, 9-19.

Tessalina, S.G., Jurdan, F. and Belogub, E.V., 2017. Significance of Late Devonian-Lower Carboniferous ages of hydrothermal suphides and sericites from the Urals Volcanic-Hosted Massive Sulphide deposits. Ore Geol. Rev., 85, 131-139.

Wu, Y.F., Evans, K., Li, J.W., Fougerouse, D., Large, R.R. and Guagliardo, P., 2019. Metal remobilization and ore-fluid perturbation during episodic replacement of auriferous pyrite from an epizonal orogenic gold deposit. Geochim. Cosmochim. Acta, 245, 98-117.

Xing, Y., Brugger, J., Tomkins, A. and Shvarov, Y., 2019. Arsenic evolution as a tool for understanding formation of pyritic gold ores. Geology, 47(4), 335-338.

Yao, X. 2021 Experimental studies on the formation of pyrite and marcasite and the mechanisms of arsenic Incorporation. Ph.D. thesis, Murdoch University, Perth, Australia.

Yao, X., Xia, F., Deditius, A.P., Brugger, J., Etschmann, B.E., Pearce, M.A. and Pring, A., 2020. The mechanism and kinetics of the transformation from marcasite to pyrite: in situ and ex situ experiments and geological implications. Contr. Mineralogy and Petrology, 175(3), 1-25

Received on: 24-09-2024; Revised on: 10-03-2025 ; Accepted on: 12-03-2025